

# Patterns of contaminant transport in a layered fractured aquifer

William J. Gburek<sup>\*</sup>, Gordon J. Folmar

*Pasture Systems and Watershed Management Research Laboratory, USDA-ARS, Pasture Lab Building,  
University Park, PA 16802 USA*

Received 2 April 1997; accepted 6 November 1998

---

## Abstract

We investigated patterns of contaminant transport within the layered and fractured aquifer of a 7.3-km<sup>2</sup> upland agricultural watershed in east-central Pennsylvania, USA. Geometry and hydraulic properties of the aquifer had been characterized by field testing and model calibration. These results were extended to simulate flow pathways and patterns of contaminant transport in both areal and cross-section formats within the watershed. The analyses indicated that the ground water flow system at the larger watershed scale is comprised of smaller units of subsurface flow which are self-contained at the scale of first- or second-order streams. For this scale subwatershed or larger, contaminant inputs to ground water from the mix of land use within the subwatershed should translate directly to the quality of nonstorm streamflow. For illustration, recharge water quality from typical land-use distributions were combined with a simple model of contaminant transport to simulate nitrate concentration patterns in ground water in a cross-section format. Land use in the vicinity of the drainage divides between streams was found to control ground water quality within the deeper layers of the aquifer, while land use over the remainder of the watershed area affected water quality only within the shallower layers of the aquifer. Streamflow nitrate data collected during a baseflow survey on the watershed were examined in context of these simulations and found to support the conclusions. Results of the study demonstrate the potential for localized contamination of ground water and nonstorm streamflow by agricultural land use, as well as the potential for managing stream quality and minimizing contamination within targeted zones of the ground water by controlling land use position. © 1999 Published by Elsevier Science B.V.

*Keywords:* Hydrology; Ground water; Watersheds; Aquifer; Fractures; Flow lines; Recharge

---

---

<sup>\*</sup> Corresponding author. Tel.: +1-814-863-8759; fax: +1-814-865-2058; e-mail: wjg1@psu.edu

## 1. Introduction

The rural population of the northeastern USA relies almost entirely on ground water for water supply. Streamflow from upland watersheds of the Northeast is derived primarily from these same subsurface sources. To evaluate effects of agricultural land use on ground water, the subsurface must be characterized locally to determine patterns of water quality within the ground water body, and at the watershed scale where ground water provides the major source of streamflow.

Nonglaciaded watersheds of the Northeast are commonly underlain by bedrock which is severely fractured and weathered at shallow depths as a result of stress-relief fracturing (Ferguson, 1967; Wyrick and Borchers, 1981). The highly conductive shallow fractured layer is a water transfer zone of major importance, influencing both hydrology and water quality dynamics within these watersheds. It can support a lateral saturated flow component which contributes directly to upland springs, seeps, and streamflow, and also supplies recharge to the deeper aquifer. Over most of the watershed, water quality within the shallow fractured layer is affected directly by overlying and immediately upgradient land use.

We have made substantial progress in understanding the hydrogeology of this layered fractured aquifer through field-based characterization of its geometry and hydraulic properties and model-based investigations of its flow dynamics. Here, we extend these investigations to consider the influence of the layered fractured hydrogeology on contaminant transport within the upland watershed setting.

## 2. Study area

WE-38 (Fig. 1) is a 7.3-km<sup>2</sup> subwatershed of East Mahantango Creek within the Susquehanna River Basin about 40 km north of Harrisburg, PA, USA. It is typical of upland agricultural watersheds of the nonglaciaded, folded and faulted Appalachian Valley and Ridge Physiographic Province. Land surface elevation ranges from about 230 to 490 m (msl) and climate is temperate and humid. Average annual precipitation is approximately 1090 mm and average annual streamflow about 460 mm. Mature forest covers the dominant ridge at the north, while cropland, pasture, and small woodlots dominate the rolling hills of the watershed's interior. Farming activities are primarily dairy, poultry, and cash cropping.

Shallow residual soils (< 1.5 m), mostly silt loams, cover the underlying bedrock which consists of two formations. The Trimmers Rock formation (Late Devonian) is predominantly shale and outcrops at the watershed outlet (south) in a near-horizontal position. The overlying Catskill (Late Devonian–Early Mississippian) consists of interbedded shales, siltstones, and sandstones, and becomes increasingly coarse-grained to the north. Dip of the Catskill strata increases to about 30° where a relatively pure quartz–sandstone–conglomerate outcrops to form the northern watershed divide (Trexler, 1964).

Rainfall, streamflow, and meteorologic data have been collected on WE-38 since 1967, and ground water data since 1972 (Fig. 1). Since 1967, there has also been

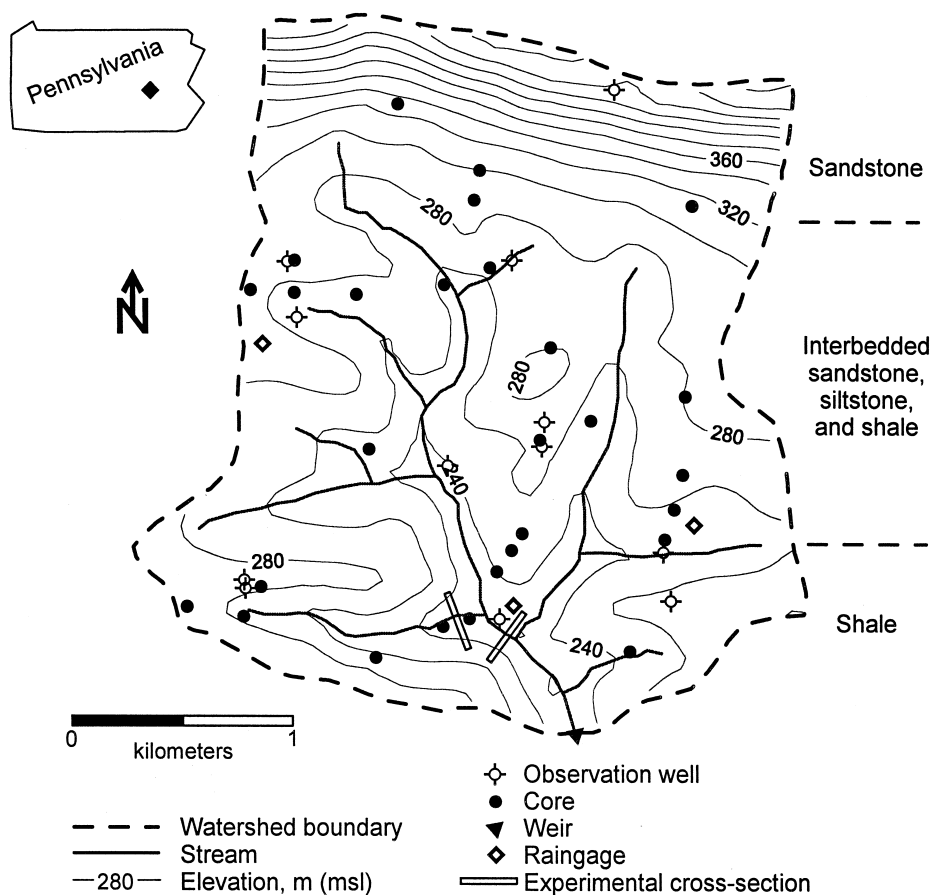


Fig. 1. Watershed WE-38 location, topography, and general hydrologic monitoring instrumentation.

continuing sampling and analysis for characterization of precipitation, soil water, surface runoff, streamflow, and ground water quality. Details of geology, soils, land use, and generalized patterns of nutrient export from WE-38 can be found in Cline (1968), Pionke and Urban (1985), and Pionke et al. (1996).

### 3. Background

#### 3.1. Aquifer characterization and ground water flow

Generalized findings of past hydrogeologic research within WE-38 relevant to the work presented here are: ground water return flow accounts for 60–80% of annual streamflow (Gburek et al., 1986; Pionke et al., 1996); water table topography exhibits steep gradients related directly to surface topography with major ground water divides

being coincident with topographic divides; and well yields decrease substantially below depths of about 90 m (Cline, 1968, Urban, 1977). Gburek and Urban (1990) investigated the hydrologic effects of shallow fracturing in two near-stream experimental cross-sections (Fig. 1). They presented local geometry of the layered fractured aquifer from rock coring and demonstrated its effects on equipotential patterns and ground water quality in the near-stream zone. Urban and Pasquarell (1992) combined results of seismic investigations and hydraulic testing of coreholes to demonstrate an internal consistency in seismic velocity and hydraulic conductivity ( $K$ ) within WE-38.

Gburek et al. (1998) combined all observations and data from these studies—230 individual seismic transects having a total length of over 9100 m, 29 rock cores drilled to a maximum of 30 m, and 132 3-m interval hydraulic packer tests—to characterize the relationships between seismic depth and velocity, fracture frequency, and  $K$  over WE-38. Using layer geometry derived from the coring and seismic testing, they also determined  $K$  values for the characteristic aquifer layers by calibrating a Visual MODFLOW (Waterloo Hydrogeologic, 1996) simulation of the ground water flow system under a springtime steady-state recharge of  $3.0 \text{ mm day}^{-1}$  to observed ground water levels at 40 observation points. Finally, they determined specific yield ( $S_y$ ) values of the layers by calibrating the ground water model to an observed master baseflow recession. The aquifer geometry, hydraulic properties, and flow field simulations reported by Gburek et al. (1998) provide the basis for the current study, so their general findings are summarized here, and the specific results are shown in Table 1.

Gburek et al. (1998) found a strong pattern of increasing seismic velocity with depth and a grouping of both velocity and layer depth by seismic layer. In general, all seismic layers sampled were found to be laterally consistent for the 9000+ m of seismic transects. Visual examination of the rock cores supported the four-layer geometry indicated by seismic testing. Based on the cores and the seismic results, they referred to

Table 1  
Summary of aquifer geometry and hydraulic properties for WE-38 (adapted from Gburek et al., 1998)

| Property   | Seismically defined layer |                  |                      |                  |
|--|---------------------------|------------------|----------------------|------------------|
|  | Overburden                | Highly fractured | Moderately fractured | Poorly fractured |
| Depth interval, m  | 0.0–2.4                   | 2.4–11.0         | 11.0–22.4            | 22.4–90          |
| Seismic velocity, $\text{m s}^{-1}$  | 460                       | 2350             | 3840                 | 5320             |
| Fracture frequency, fractures $\text{m}^{-1}$                                  | n/a                       | 30+              | 20                   | < 5              |
| <i>Hydraulic conductivity (<math>K</math>), <math>\text{m day}^{-1}</math></i> |                           |                  |                      |                  |
| Regional aquifer testing (Cline, 1968)   | n/a                       | n/a              | n/a                  | 0.03             |
| Packer testing (Urban and Pasquarell, 1992) <sup>a</sup>                       | 6.0                       | 1.14             | 0.41                 | 0.38             |
| Near-stream study <sup>a</sup> (Gburek and Urban, 1990)                        | n/a                       | 2.2e 0.6w        | 0.6e 0.3w            | n/a              |
| Model calibration (Gburek et al., 1998)  | 20.0                      | 5.0              | 0.1                  | 0.01             |
| <i>Specific yield (<math>S_y</math>)</i>                                       |                           |                  |                      |                  |
| Regional aquifer testing (Cline, 1968)   | n/a                       | n/a              | n/a                  | 0.0001           |
| Model calibration (Gburek et al., 1998)  | 0.01                      | 0.005            | 0.001                | 0.0001           |

<sup>a</sup>Geometric means of all data.

<sup>b</sup>e and w indicate east and west cross-sections.

the four layers as: (1) soil or overburden, (2) highly fractured, (3) moderately fractured, and (4) poorly fractured or regional aquifer. Here we will use the general term, 'shallow fracture zone', to indicate the top three layers of the aquifer.

Gburek et al. also observed two sets of fractures within the cores, one parallel to the bedding planes and the other roughly orthogonal thereto. Bedding-plane fractures were somewhat more numerous, but relative frequencies of fractures within each set were not quantified. They assumed sufficient fractures within each set to support an initial assumption of isotropic media for all layers.

Variabilities of each parameter (depth, velocity, fracture frequency,  $K$ , and  $S_y$ ) associated with each characteristic layer were indicative of the properties of fractured rock within WE-38 at the scale of the particular sampling or characterization methodology. Packer and slug tests, because of the relatively small aquifer volume sampled, represented the extremes of aquifer properties effective at the small scale, i.e., very large  $K$ s from locally high concentrations of fractures, or very low  $K$ s from a local absence of fractures. The geometric mean of these values, generally thought to be most representative of an aquifer as a unit, still reflected the more localized aquifer properties. Conversely, the watershed-scale model calibration represented bulk aquifer properties which are a function of the larger scale extent of fracturing and interconnectedness of the fracture system. Thus, the packer and slug test field data were comparable only to model calibration values in the highly and moderately fractured layers, where the larger scale flow field was controlled by a higher density of interconnected fractures. Where the flow field was controlled by a more sparse and less interconnected fracture system, as in the poorly fractured layer, the regional scale aquifer testing technique (the pumping test) better characterized the watershed-scale controls on the ground water flow field and was more related to their calibrated values.  $S_y$  values from their calibrations, except for that of the poorly fractured layer, were unable to be compared to field data because none are available for the shallower fracture zones. Calibrated  $S_y$  for the poorly fractured layer compared favorably to the range of values reported by Cline (1968) from pumping tests over the Mahantango Watershed, and to model results presented by Gerhart (1984).

There were no obvious patterns or trends to the seismic velocity-layer depth-fracture frequency– $K$  relationships within WE-38 related to direction, rock type, or topographic setting. The most obvious feature of the seismic data was large standard deviations relative to the mean values, especially in layer depths. Gburek et al. attempted to explain the variabilities using a variety of techniques (e.g., simple contouring and geostatistics) related to topography and generalized geology, but no spatial patterns were found. Both the depths and the velocities of the four characteristic layers were approximately normally distributed, so their working hypothesis was that since the variations were random, the best estimate of aquifer layer depths and hydraulic properties over the watershed were their mean values.

### 3.2. Water quality (nitrates)

Nitrates in the Susquehanna River have been identified as a major contributor to eutrophication within Chesapeake Bay (EPA, 1983). EPA (1996) also maintains that agriculture is the major source of nutrients associated with eutrophication in 50% of the

lakes and 60% of the river miles determined to have impaired water quality. Thus, knowledge of processes controlling nitrate contamination of ground water and resultant streamflow from upland watersheds is critical. It is generally accepted that a major source of nitrates to ground water of rural upland watersheds is agriculture, but studies relating agricultural land use to ground water quality rarely consider the more complete interrelationships between land use, ground water quality, and the quality of streamflow leaving the watershed.

Pionke and Urban (1985) showed that within WE-38, long-term nitrate losses below the root zone approximate those in streamflow at the watershed outlet, suggesting that the below-root-zone flow system is mainly a zone of transmission. They also found that nitrate–nitrogen ( $\text{NO}_3\text{-N}$ ) concentrations in wells representing the aquifer of WE-38 between 10 and 60 m depth were lowest beneath forest at the major divide in the north, averaging  $0.7 \text{ mg l}^{-1}$ , highest under cropland in the mid-watershed position, averaging  $4.7 \text{ mg l}^{-1}$ , and low again near the watershed outlet (south), averaging about  $1.3 \text{ mg l}^{-1}$ . Samples from piezometers in the near-stream experimental cross-sections (Gburek and Urban, 1990) showed  $\text{NO}_3\text{-N}$  concentrations in the shallow ground water to be related directly to overlying land use; values ranged from  $6.8$  to  $22.6 \text{ mg l}^{-1}$  under a corn-based strip-crop rotation to less than  $1.0 \text{ mg l}^{-1}$  under unmanaged meadow. Concentrations in the ground water directly under the streams and in the streams themselves reflected the mixing of these concentration extremes from both sides of the channel.

Schnabel et al. (1993) simulated nitrate levels at the WE-38 outlet using a two-layer mixing model having higher  $\text{NO}_3\text{-N}$  concentrations in the shallower layer and lower concentrations at depth. This model duplicated longer term patterns of nitrate export from WE-38, higher and more variable concentrations during periods of high flow when the stream is more influenced by flows from the shallower layer, and lower more stable concentrations during periods of baseflow when the deeper layers with lower nitrate concentrations more related to overall land use dominate streamflow. A one-time late-summer sampling of baseflow quantity and quality throughout WE-38 in 1992 (unpublished data) showed that first-order streams originating at the base of the forested ridge at the north had  $\text{NO}_3\text{-N}$  concentrations typically less than  $1.0 \text{ mg l}^{-1}$ .  $\text{NO}_3\text{-N}$  concentrations in the first- and second-order streams draining the dominantly agricultural subwatersheds along the east and west boundaries of WE-38 were substantially higher, up to  $20 \text{ mg l}^{-1}$  where they enter the main channels. Aggregation of all watershed land uses resulted in  $\text{NO}_3\text{-N}$  concentrations in baseflow of about  $5 \text{ mg l}^{-1}$  in the main channels from about mid-watershed position to the watershed outlet, approximately the same concentration reported by Pionke et al. (1996) for long-term baseflow.

### 3.3. Study objectives

Water quality modeling efforts in support of management and/or regulation should incorporate the major factors controlling chemical loads generated by contributing watersheds: spatially distributed water and chemical recharge to ground water, subsurface flow dynamics and associated patterns of contaminant transport, and the relationship between subsurface flow and the streams draining the watersheds. Objectives of the

work reported here were to investigate the potential for hydrogeologically based ground water modeling to help us interpret observed patterns of nitrate concentrations in the ground water and streamflow, and also provide a modeling framework to guide future research. We examined flowpath patterns at the watershed scale to quantify the general subsurface flow system. Flowpaths within representative cross-sections at watershed and local scales were simulated to more closely examine patterns of flow resulting from the combination of topography and influence of the layered fractured aquifer. We also simulated nitrate concentration distributions resulting from observed and hypothetical patterns of land use. Finally, we compared results from these simulations to baseflow data collected within the watershed, and discussed management-related implications of the findings.

#### **4. Flowpath simulation: areal format**

##### *4.1. Methodology*

Visual MODFLOW (Waterloo Hydrogeologic, 1996), commercially available ground water modeling software combining MODFLOW (McDonald and Harbaugh, 1988) and MODPATH (Pollock, 1989) with a graphical user interface, was the basis for all modeling. MODFLOW can simulate saturated flow within layered water-table aquifers like those of WE-38 in either a two- or three-dimensional format. Block-centered finite-difference approximations are used to solve the ground water flow equations, and recharge is assumed to be applied directly to the water table.

MODPATH/Visual MODFLOW can simulate and display pathways followed by particles introduced into the flow field produced by a MODFLOW simulation. Flowpaths are determined by tracking the trajectories of the particles via interpolation of the block-centered flow values. The particles are considered soluble, noninteractive, and nontransformable; i.e., they move as a water molecule. Mixing because of molecular diffusion or mechanical dispersion is ignored. Finally, travel times along flowpaths can be portrayed based on mass flowrates and effective porosity.

##### *4.2. Results*

The Visual MODFLOW simulation of the WE-38 ground water flow system under springtime steady-state recharge of  $3.0 \text{ mm day}^{-1}$  described previously (Gburek et al., 1998) was used as the basis for our investigation of the areal-format watershed-scale flowpaths. Land surface topography was digitized and gridded from the Valley View, PA U.S. Geological Survey 7.5-min quadrangle using SURFER (Golden Software, 1995), the topographic watershed boundary of WE-38 defined the impermeable lateral boundaries of the model, and  $100 \times 100 \text{ m}$  cells were used to represent the watershed interior. Aquifer geometry was based on Table 1. Land surface elevation of each cell was reduced by 2.4, 11, and 22.4 m to define the bottom of the overburden, highly fractured, and moderately fractured model layers, respectively, based on the assumption

derived from the seismic sampling that the layers are uniform in depth over the watershed (Gburek et al., 1998). These depths were also set as the bottom boundaries for the top three computational cells. The impermeable bottom boundary for the model was assumed to be a plane sloping upward from south to north at 0.015 (the general land surface slope from the weir to the base of the ridge at the north of the watershed), with the plane positioned at 90 m below the land surface at the point of the watershed outlet (Cline, 1968). The bottom geologic layer (poorly fractured) was divided into three computational cells, two of 20 m thickness beginning immediately below the bottom of the moderately fractured layer at 22.4 m depth, and one extending from these to the bottom impermeable boundary of the flow system. Model cells containing any part of the channel network were specified as MODFLOW stream cells. Channel bottom elevation within each cell was determined from the contour map, and we assumed minimal restriction to flow from ground water to the channel by assigning a high value of conductance to each stream cell (Gburek et al., 1998).

Values of  $K$  used for the four characteristic fracture layers were those termed 'Model calibration' in Table 1, and they were assumed uniform over the watershed within each aquifer layer. There are questions regarding applicability of a continuum-based model, such as MODFLOW, to a flow system controlled by fracturing, but it has been shown (Long et al., 1982; Peters and Klavetter, 1988; Khaleel, 1989; Gburek et al., 1998) that such modeling can be successful when fracture density is relatively high compared to the scale of the problem being investigated. Fracture frequencies within the WE-38 aquifer range from over 30 to less than  $5 \text{ m}^{-1}$  (Table 1), and when these frequencies are compared to grid spacing and layer depths used in the modeling efforts presented here, the continuum approach appears reasonable. The other caveat on all simulations is that a fracture system may introduce anisotropy in aquifer parameters (Lee et al., 1992). We have no quantitative evaluation of the potential degree of anisotropy in the fracture layers of the WE-38 aquifer, but based on fracture geometry observations described previously, we assumed isotropy in all simulations.

Fig. 2 shows the pattern of flowpaths within the steady-state high-recharge ground water flow field resulting from particles being introduced at the surface of the water table in the center of most 100-m square cells. The figure is a plan view of the three-dimensional flowpaths moving through all model layers; i.e., flowpaths shown have vertical components into and through the ground water body before returning to the water table to discharge to a stream node (where each flowpath ends). In plan, the flowpaths generally follow water table gradients which are typically a subdued version of the land surface. They emerge from the ground water either directly to the nearest stream or, at most, to the nearest downgradient stream of the next highest order. There are no significant instances of flowpaths passing beneath one stream to emerge to another, thereby forming nested subsurface flow systems as presented by Toth (1963). Some flowpaths do cross first-order tributaries which are ephemeral in nature, but in total, the figure indicates only the existence of small-scale, self-contained subsurface flow fields.

Note that many of the flowpaths, once in the vicinity of the channel, turn parallel to the channel and remain within the ground water for short distances before emerging to the stream. Because all internal geologic layer boundaries are defined as parallel to the

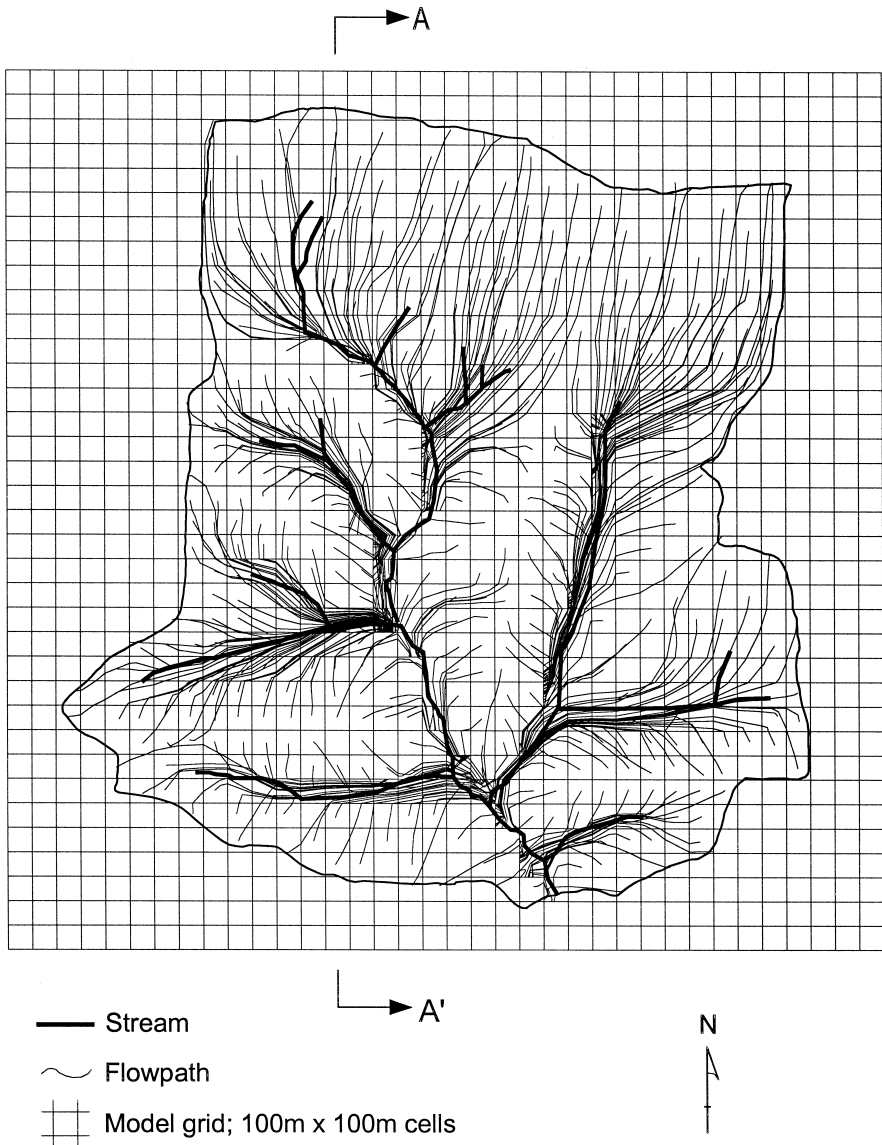


Fig. 2. Flowpaths initiated at water table in center of MODFLOW cells under late-spring/early-summer steady-state recharge.

land surface, a V-shaped zone of high  $K$  exists under all streams (i.e., a reflection of land surface topography). This results in a subsurface flow component parallel to each stream as reflected by the pattern of the flowpaths, a phenomenon also noted by Gburek and Urban (1990) in their cross-section investigations.

## 5. Watershed-scale simulations: cross-section format

### 5.1. Methodology

Details of flowpath patterns and their effects on ground water and stream quality can be more easily visualized and evaluated in a two-dimensional format. The watershed-scale cross-section A–A' in Fig. 2 is transected by four streams nearly orthogonal to the section, and further, most flowpaths contributing to these streams in the vicinity of A–A' are parallel to the plane of the section. Thus, we assume this cross-section to be a two-dimensional representation of the three-dimensional watershed-scale ground water flow system; it contains the same range of topography, multiple flow systems, and multiple streams as does the complete watershed.

Visual MODFLOW was applied to this cross-section (Fig. 3) using the same internal aquifer geometry, hydraulic properties, computational cell geometry, and recharge as in the watershed-scale flowpath simulations. For external boundaries, both ends of the cross-section were assumed impermeable, the impermeable bottom was that of the areal simulation, and outlets for flow from the section were four stream cells located in the uppermost layer at the positions of the streams crossing the section. This is a two-dimensional simulation, so the assumption inherent in the flow field solution is that all flow occurs within the cross-section. Simulated water table topography within the section compared favorably to water levels measured in wells along and near it under similar recharge conditions.

### 5.2. Results

Fig. 3 shows selected flowpaths initiated at the water table in the vicinity of the topographic divides; these are the most critical positions for defining the overall flow field in strongly layered systems (Selim, 1987; Gburek et al., 1991). The bottom of the moderately fractured layer at 22.4 m depth is shown in Fig. 3 as a dashed line. Most

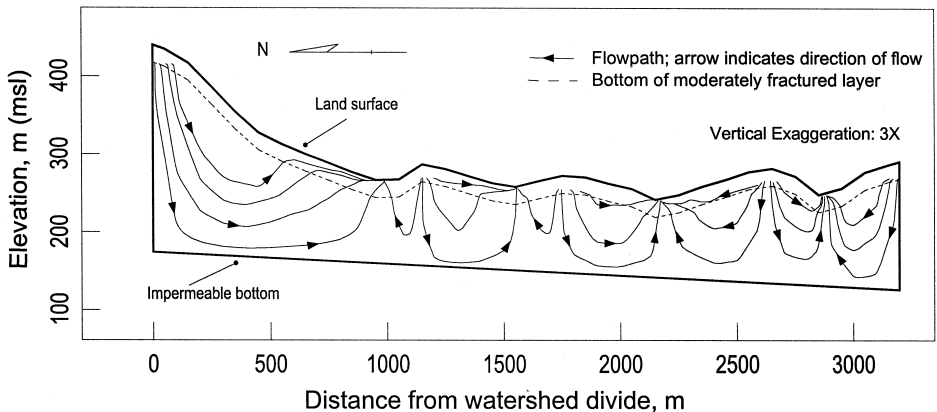


Fig. 3. Flowpaths within the watershed-scale cross-section A–A' (Fig. 2) under steady-state recharge.

obvious is the fact that no nested subsurface flow systems appear within this cross-section, i.e., no flowpaths originating at one divide pass under the nearest stream to emerge at a stream lower in elevation. All flowpaths beginning near the major divides at each end of the section, as well as those beginning near the minor interior divides, terminate at the nearest stream. In some cases, even though the flowpaths are begun near the divides, they remain entirely within the shallow fracture zone, i.e., those within the portions of the cross-section 1100 to 1500 m from the divide and 2600 to 2200 m from the divide. This figure also shows how the higher  $K$ s within the shallow fracture zone act similar to a drain, bringing flowpaths from the deeper portions of the cross-section into the fracture zone before they arrive at the stream, i.e., the two shallower flowpaths shown within the portion of the section 0 to 1000 m from the divide. The vertical flow components shown in Fig. 3 are those unable to be portrayed in Fig. 2.

Theoretically, there should be some nesting of flow systems within this cross-section geometry because of different elevations of the four streams. More detailed analysis of the section was done to examine the possibilities for their existence. By introducing an extremely large number of particles spread across the cells adjacent to the major divides, we were able to generate a limited number of flowpaths positioned very near the impermeable boundary of the section that bypassed the nearest stream to emerge at another downgradient. However, the amount of flow represented by these flowpaths is insignificant compared to flow through the entire cross-section.

## 6. Local-scale simulations: cross-section format

### 6.1. Methodology

Fig. 3 provides a cross-section based portrayal of flowpaths at the watershed-scale, but a local-scale cross-section (between 1100 m to 2700 m from the watershed divide) can be abstracted from the larger section and examined in further detail. We are able to remove this local section from the watershed-scale section and replace its open ends with impermeable boundaries because of approximate flow field symmetry at these subwatershed divides; i.e., Fig. 3 shows no lateral flow components across these divides. The local-scale cross-section includes two crossing streams and three interstream areas (Fig. 4). For the flow field simulation within this section, all boundaries, hydraulic properties, and internal layer geometry were as in the watershed-scale cross-section simulation. However, grid spacing in the horizontal was reduced to 30 m for better resolution of the flow field, flowpaths, and evaluation of effects of land use distribution on nitrate concentrations within the section. Both 'subwatersheds' at the ends of this local-scale cross-section are roughly the dimensions of typical divide-to-stream cross-sections within the valley-floor area of WE-38, approximately 400 m in length and 40 m in relief.

### 6.2. Flowpaths

Ground water flow within this local-scale cross-section was modeled under the 3.0 mm day<sup>-1</sup> springtime recharge rate used previously, and also under 0.3 mm day<sup>-1</sup>, a

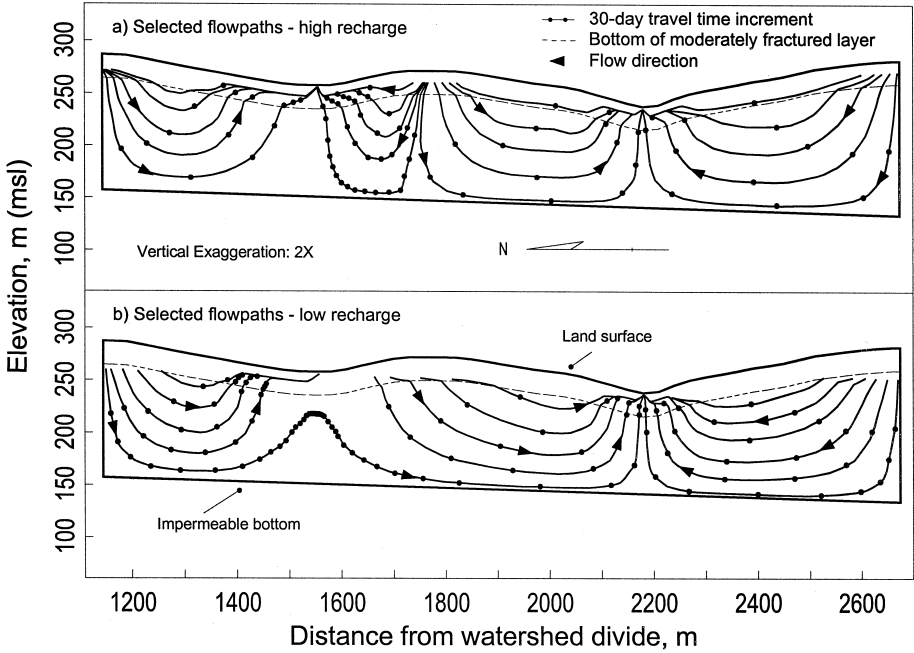


Fig. 4. Flowpaths and associated travel times within the local-scale cross-section under high and low steady-state recharge rates.

rate more characteristic of late-summer/early-fall conditions on the watershed. Flowpaths and associated patterns of contaminant transport under these extremes show the range of variations expected over the year. Selected flowpaths within these high- and low-recharge flow fields are shown in Fig. 4a and b, respectively. As before, all flowpaths were initiated at the water table within cells at or near water table divides. Ground water tables were not shown to avoid unnecessary complication of the figure, but their position can be inferred from the approximate beginning points of the flowpaths. In the high-recharge case (Fig. 4a), the flowpaths resulting range from those that parallel the impermeable boundaries of the cross-section to some remaining entirely within the shallow fracture zone. At this increased level of resolution of the flow field, there is still no indication of nested subsurface flow systems under high-recharge conditions.

The flowpath pattern resulting from the low-recharge regime (Fig. 4b) exhibits notable differences. Now, one flowpath beginning near the divide at the north (~ 1200 m from the divide on the *x*-axis) passes under the northernmost stream at about 1600 m to emerge at the stream in the south because the ground water divide that was between the two streams under high-recharge conditions (~ 1750 m) has disappeared. The northern stream is now a point of partial discharge for ground water from its north, and since it is only partially effective in draining this portion of the cross-section, some underflow component must occur. The southern stream becomes the ultimate point for subsurface discharge from the cross-section. Under high-recharge conditions, the simula-

tions indicate that the northern stream receives about 40% of the outflow from the entire section and the southern stream 60%, roughly proportional to the recharge areas defined by water table divides as well as topographic divides. Under low-recharge conditions though, the northern stream receives slightly less than 30% of total outflow from the section, approximately the proportion of land area in the cross-section to its north. The area to the south contributing ground water discharge to this stream under high-recharge conditions ( $\sim 1600\text{--}1750$  m), and the small amount of underflow represented by the flowpath shown (originating within 5 m of the divide), account for the 10% difference. This pattern of underflow suggests that there may be problems with extracting the local-scale cross-section from that of the watershed scale based on the assumption of impermeable lateral boundaries at the intermediate watershed divides. We re-examined the watershed-scale cross-section for the possibility of underflow under low-flow conditions, and found that while some does exist, it is not a major flow component, thereby justifying extraction of the local-scale cross-section.

The isolated flow system at the southern end of the section shows another important effect of lower recharge—flowpaths beginning in similar positions tend to go deeper into the aquifer. Under high recharge, the flowpath beginning approximately 70 m from the southern divide remains entirely within the fracture layer all the way to the stream, but in the low-recharge case, flowpaths originating over 100 m from this divide dip into the deeper aquifer before emerging to the stream. The lesser total flow moving through the aquifer under low-recharge conditions is more easily accommodated by the deeper portions of the aquifer. This results in deeper and more extensive penetration of the flowpaths into the aquifer and consequently, potential for transport of contaminants deeper into the subsurface flow system.

### 6.3. Travel times

Travel times developed by the MODPATH option of Visual MODFLOW are shown on the flowpaths of Fig. 4a and b by dots spaced at 30-day time increments. Travel times are estimated by inclusion of effective porosity in the flow equations to calculate within-pore velocity along the flowpaths. The matrix material of the bedrock underlying WE-38 has very low  $K$  ( $< 3 \times 10^{-4}$  m day $^{-1}$ ) and effective porosity ( $< 0.005$ ) (Gburek and Urban, 1990). Thus, we have hypothesized that  $K$  and effective porosity of the fracture network control ground water velocities within the flow field (Gburek and Urban, 1990; Gburek et al., 1998). Because the WE-38 aquifer is unconfined over the depths we are modeling (Cline, 1968),  $S_y$  values from Table 1 were assumed equal to the effective porosity for input to MODPATH to perform travel time simulations. Note that we have not considered travel times in the unsaturated portion of the subsurface flow system.

In Fig. 4a (high recharge), travel times along the longer and deeper flowpaths range from  $> 150$  days in the south to  $> 210$  days in the north. Travel times along the shallowest flowpaths range from  $> 30$  to  $> 60$  days. The general conclusion from these travel time simulations is that once a contaminant is introduced into the ground water under high recharge conditions, its effects may be felt throughout much the shallower ground water zones and in the receiving stream within the time scale of a year or less,

even if introduced near a local ground water divide. Additionally, there are major subsurface flowpaths from water table to stream having travel times that may move a contaminant through the saturated flow system within the time scale of months, i.e., those that remain in the high-conductivity low-porosity shallow fracture zone.

The low-recharge regime alters travel times dramatically. Those along flowpaths in the southern flow system are  $\sim 100$  days longer than their high-recharge counterparts. The middle and northern flow systems exhibit the greatest differences in travel times (as in flowpath patterns) because of the reduced hydraulic gradients from divide to stream under low-recharge conditions. Flowpath velocities slow dramatically as they approach the stream because of decreased gradients as evidenced by lower ground water tables, and associated decreased flowrates as evidenced by decreased streamflow. Increased  $S_y$  in the shallow aquifer in the near-stream zone also decreases velocity along the flowpaths; the same effect is observed to a lesser extent in the high recharge simulation. Finally, travel time along the flowpath bypassing the northern stream is quite long, over three years from ground water table to stream.

There are two caveats on these travel times, however. First, the simulations in Fig. 4a and b are extremes of annual watershed performance, springtime high recharge and summertime low. Flowpath patterns over the course of the year will vary between these, so travel times on an annual basis will be somewhere between the extremes presented. Second, and perhaps most critical to interpretation of our results, the travel times presented are based strictly on values of  $S_y$  determined by calibration of ground water model results against observed well data and baseflow recessions (Gburek et al., 1998), except for that of the poorly fractured layer (Table 1). These calibrated values were supported by another modeling investigation in the same geologic region (Gerhart, 1984), but there are no independent field-based verifications of the  $S_y$  values for the zone of fracturing down to 22.4 m. Further, we assumed these  $S_y$  values equivalent to effective porosity. There was no consideration given to possible effects of such factors as degree of interconnectedness of the fractures or tortuosity of flowpaths resulting from configuration of the fracture network, both important in characterizing the porosity of fractured aquifers that controls contaminant transport. These factors would tend to increase travel times through the fracture system, but the possible extent of increase in our situation will remain unknown until appropriate field testing can be done.

#### *6.4. Nitrate concentration patterns*

We simulated effects of land use distribution on patterns of nitrate concentration within the layered fractured aquifer by combining characteristic root-zone percolate nitrate concentrations with a simple contaminant transport model originally developed to simulate steady-state transport of a dissolved and conservative chemical within MODFLOW ground water flow simulations (Gburek et al., 1991). Nitrate can be assumed soluble and conservative once introduced into the ground water flow system. The transport model assumes plug flow between cells, complete mixing within each cell, and uses spatially variable percolate water quality as input. The steady-state solution minimizes problems with numerical dispersion inherent in such a model, and the cell sizes used, grading from smaller at shallower depths where more variability is expected, to larger at the bottom of the aquifer where concentration gradients are more uniform,

are appropriate to the scale of the problem and do not limit interpretation of our results. The nodal arrays of concentrations produced by the transport model were contoured by the SURFER software to produce all  $\text{NO}_3\text{-N}$  contour plots shown.

For model input, we used nitrate concentrations typical of recharge from the general land use categories on our watershed cross-section. Ground water recharge from forest or unfertilized grass land use was assumed to contain  $1.0 \text{ mg l}^{-1}$   $\text{NO}_3\text{-N}$ , and that from typically fertilized crop rotation  $8.0 \text{ mg l}^{-1}$  (Pionke and Urban, 1985; Gburek and Urban, 1990). Continuous corn land use was assumed to provide a  $\text{NO}_3\text{-N}$  concentration of  $20.0 \text{ mg l}^{-1}$  in recharge (Jemison and Fox, 1994; also unpublished shallow ground water sampling within WE-38).

Four nitrate concentration simulations were produced using the local-scale cross-section flow fields from Fig. 4, actual land use on the watershed under high and low recharge rates (Fig. 5a and b), and two hypothetical patterns of land use under high recharge (Fig. 5c and d). Under high recharge and actual land use (Fig. 5a), forest at the southern end of the cross-section maintains ground water in the deeper zone of the aquifer at  $1.0 \text{ mg l}^{-1}$   $\text{NO}_3\text{-N}$  to the position of the channel. The crop rotation land use (2200–2400 m from the divide) primarily affects ground water within the shallow fracture zone. Conversely,  $\text{NO}_3\text{-N}$  concentrations in the deeper ground water of the northern end of the section are dominated by the overlying crop land use ( $8.0 \text{ mg l}^{-1}$   $\text{NO}_3\text{-N}$ ). Nitrate patterns between the two streams in the center part of the local-scale cross-section are more complex. Here, the forest land use to the south of the northern stream which extends to and slightly beyond the topographic divide ( $\sim 1600\text{--}1800$  m) results in a large portion of the aquifer extending to the south having  $\text{NO}_3\text{-N}$  concentrations of  $< 2.0 \text{ mg l}^{-1}$  because the ground water divide is slightly to the north of the surface water (topographic) divide.

Fig. 5b shows the simulated pattern of ground water nitrate concentrations resulting from actual land use under low recharge. The pattern resembles that of Fig. 5a, but shows local differences. One notable difference is a feature discussed in the flowpath patterns; effects of the cropped land use toward the south of the section (2200–2400 m) extend deeper into the aquifer under the low-recharge regime. Concentrations of  $1.0 \text{ mg l}^{-1}$  were almost entirely within the fracture layer under high recharge conditions, but under low recharge, the  $1.0 \text{ mg l}^{-1}$  concentration contour is substantially below the fracture layer boundary. Nitrate concentration from the cropped land in the northernmost subwatershed is now mixed with that from forest land use beginning at about 1400 m from the divide because of the partially discharging stream and underflow. This results in concentrations under the stream of less than  $8.0 \text{ mg l}^{-1}$  as was found in the high-recharge case. The bulk of the deeper aquifer between the two streams was at a concentration  $< 2.0 \text{ mg l}^{-1}$  under high recharge, whereas under low recharge, it is between  $2.0$  and  $3.0 \text{ mg l}^{-1}$  because of flow from the crop rotation land use to the north passing beneath the stream.

Fig. 5c and d consider only continuous corn and unmanaged (forests/unfertilized grass) land uses for illustrating effects of land use positioning on ground water quality. About 35% of each interstream zone was assumed to be in continuous corn planted in a single field; this percentage is characteristic of land use distribution within WE-38. The concentration pattern shown in Fig. 5c results from the three corn fields being placed at

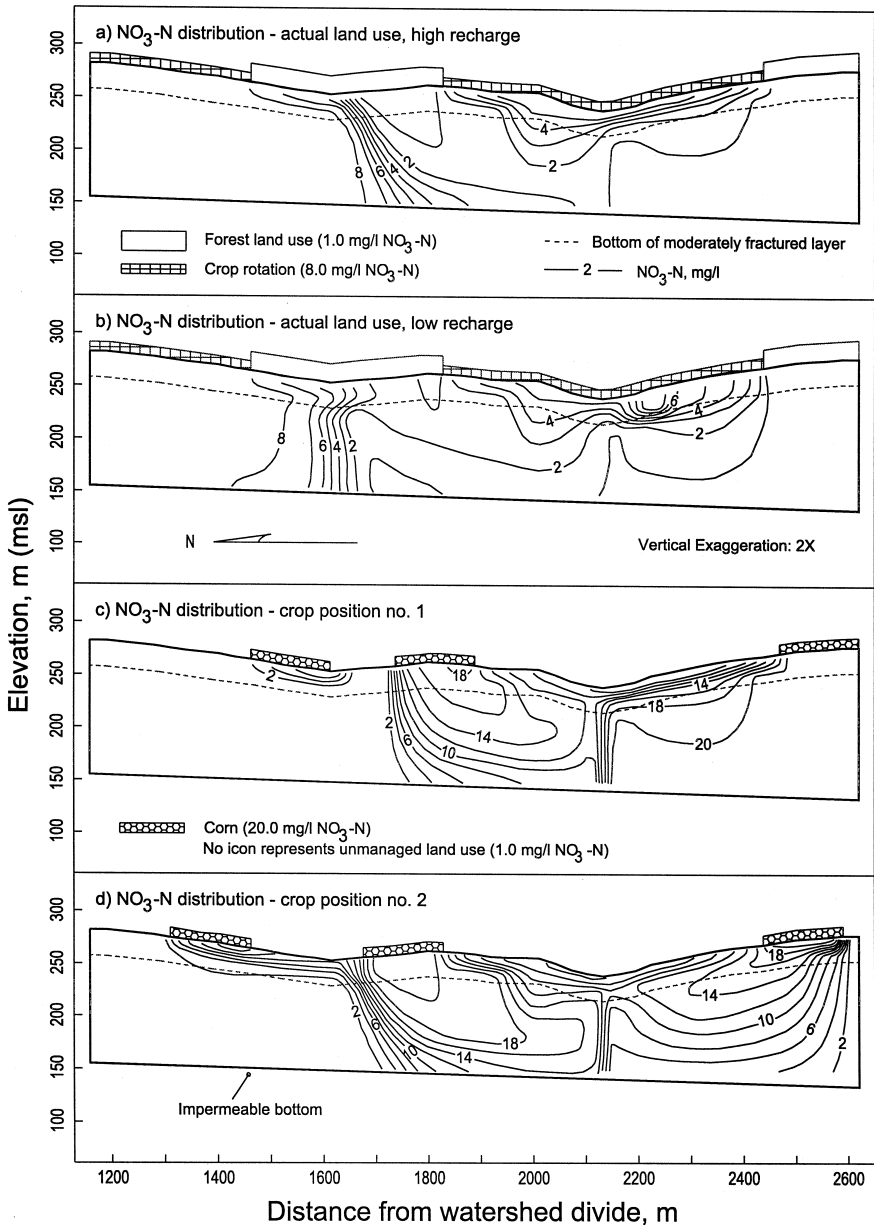


Fig. 5. Simulated patterns of NO<sub>3</sub>-N concentrations within the local-scale cross-section under actual land use for high and low recharge rates (a and b), and two hypothetical land use distributions (c and d).

the southern divide, immediately adjacent to the northern stream, and directly over the topographic divide in the middle zone, respectively. Corn land use at the divide (south) causes the aquifer adjacent to the divide to be contaminated with 20.0 mg l<sup>-1</sup> NO<sub>3</sub>-N

throughout most of its depth. Ground water within the shallow fracture zone downgradient exhibits continuing dilution of this recharge by the unmanaged land use. Effects of the contrast in  $K$  between the fracture layer and the deeper aquifer (Table 1) appear as kinks in the concentration contours as they cross the fracture layer boundary. The corn field adjacent to the northern stream affects only the shallowest part of the flow system. Here, ground water flow tends to be parallel to the land surface or upward as it converges to discharge to the stream (see Fig. 4a). Consequently, effects of overlying land use do not extend deeply into the aquifer, a condition also noted by Gburek and Urban (1990) when examining nitrate concentrations in the near-stream piezometers of the experimental cross-sections. Simulated concentrations in the ground water are much less than the  $20.0 \text{ mg l}^{-1}$  from the corn because they are being mixed with larger amounts of ground water from the unmanaged land use upslope. In the middle of the cross-section, the corn field is seen to primarily affect the ground water and stream to the south because the ground water divide is near the northern edge of the corn field.

Fig. 5d shows the concentration pattern resulting from slightly repositioning the corn fields. Moving the corn land use one node (30 m) from the southern divide reduces nitrate concentrations within the deeper aquifer to generally  $< 14.0 \text{ mg l}^{-1}$ , and also moderately reduces concentration in all downslope positions within the fracture layer. The difference between Fig. 5c and d in this portion of the cross-section illustrates the sensitivity of water quality in the deeper aquifer to distribution of land use on the recharge zone in strongly layered hydrogeology (Selim, 1987). The corn field previously adjacent to the stream (northern subwatershed) was moved midway up the slope, but still impacts only the shallow zone of fracturing in a minor way. Maximum concentrations are now about  $12 \text{ mg l}^{-1}$ , and these are only directly beneath the corn. The third field was moved entirely to the northern side of the local topographic divide, yet it continues to impact ground water to the south. In fact, this move resulted in a greater extent of contamination of ground water between the two streams; maximum nitrate concentrations in this area of the ground water body are higher as a result of the move, and the area affected by the higher concentrations is more widespread. The second position, while further off the topographic divide, places the corn land use directly over the ground water divide.

## 7. Comparison to field data

All flowpath simulations suggest that the ground water flow system at the scale of WE-38 consists of a smaller number of subsurface flow systems which are self-contained at the subwatershed scale, perhaps down to second-order streams. Nitrate data collected and analyzed during a baseflow survey on WE-38 (unpublished data) are used to test this inference. The baseflow survey, conducted in late summer of 1990, was a preliminary examination of watershed-scale controls on streamflow quantity and quality under low-flow conditions. The flow data collected at each tributary junction within WE-38 represents drainage of the aquifer with minimal influence of stormflow conditions, and corresponding nitrate concentrations represent the long-term influence of land

use over the watershed. Table 2 gives details of 15 subwatersheds within WE-38 which correspond in size and location to the variety of individual and nested subsurface flow systems indicated by the flowpaths of Fig. 2. Drainage areas of the subwatersheds, determined directly from the topographic map, range from 0.45 km<sup>2</sup> (W.T4.3) to the entire 7.3-km<sup>2</sup> WE-38. Land use distribution within each subwatershed was determined directly from detailed surveys conducted within WE-38 by ARS field personnel.

Pionke and Urban (1985) presented a nitrogen balance at the scale of WE-38, with all nitrate in recharge being sampled at the watershed outlet. They suggested that this N balance was realized because of long-term stability of land use patterns within WE-38 and the fact that the dominant shallow ground water flow system quickly translates recharge inputs from the mix of land use to the watershed outlet. Based on this and the flowpath simulations developed here, we hypothesize that nitrate in recharge from the distribution of land uses *within* the 15 subwatersheds of WE-38 (Table 2) will control nitrate concentration at each of their respective outlets. To test this, we characterized recharge NO<sub>3</sub>-N concentration for each of the land use categories in Table 2, summed the NO<sub>3</sub>-N inputs to each of the subwatersheds, and compared the results to the measured nitrate concentrations at their outlets. In addition to the three characteristic NO<sub>3</sub>-N recharge concentrations previously used (forest/unfertilized land use at 1.0 mg l<sup>-1</sup>, crop rotation at 8.0 mg l<sup>-1</sup>, and continuous corn at 20.0 mg l<sup>-1</sup>), we added a permanent pasture land use category at 10.0 mg l<sup>-1</sup> NO<sub>3</sub>-N in ground water recharge (Scholefield et al., 1993; Owens et al., 1994), and confined animal areas at 30.0 mg l<sup>-1</sup> (personal communication, R.R. Schnabel).

Table 2  
Basic data for subwatersheds within WE-38

| Site   | Drainage area, km <sup>2</sup> | Observed baseflow, l s <sup>-1</sup> | Land use distribution, percent of subwatershed area |               |                 |                   |                  | NO <sub>3</sub> -N, mg l <sup>-1</sup> |                         |
|--------|--------------------------------|--------------------------------------|---|---------------|-----------------|-------------------|------------------|--|-------------------------|
|        |                                |                                      | Forest  | Crop rotation | Continuous corn | Permanent pasture | Confined animals | Measured                               | Calculated <sup>a</sup> |
| W.6    | 1.22                           | 8.0                                  | 85  | 14            | 0               | 0                 | 1                | 2.6                                    | 2.3                     |
| W.T3.4 | 0.65                           | 3.9                                  | 56  | 41            | 3               | 0                 | 0                | 4.6                                    | 4.5                     |
| W.10   | 2.19                           | 8.6                                  | 69  | 29            | 1               | 0                 | 1                | 3.5                                    | 3.4                     |
| W.T4.3 | 0.45                           | 1.1                                  | 21  | 77            | 2               | 0                 | 0                | 15.3                                   | 16.0 <sup>b</sup>       |
| W.12   | 2.81                           | 8.6                                  | 59  | 39            | 1               | 0                 | 0                | 4.9                                    | 4.1                     |
| W.T5.3 | 0.79                           | 1.2                                  | 33  | 60            | 2               | 3                 | 3                | 8.0                                    | 6.5                     |
| W.15   | 3.93                           | 14.6                                 | 51  | 46            | 1               | 1                 | 1                | 5.0                                    | 4.8                     |
| W.T6.3 | 0.58                           | 1.4                                  | 46  | 53            | 0               | 1                 | 0                | 6.2                                    | 4.8                     |
| W.17   | 4.57                           | 22.3                                 | 50  | 48            | 1               | 1                 | 1                | 5.2                                    | 4.8                     |
| E.1    | 0.71                           | 7.3                                  | 87  | 13            | 0               | 0                 | 0                | 1.5                                    | 1.9                     |
| E.6    | 1.48                           | 5.4                                  | 53  | 46            | 0               | 2                 | 0                | 3.5                                    | 4.4                     |
| E.T1.5 | 0.67                           | 1.4                                  | 15  | 74            | 6               | 4                 | 0                | 7.7                                    | 7.7                     |
| E.9    | 2.31                           | 6.9                                  | 39  | 57            | 2               | 3                 | 0                | 3.6                                    | 5.6                     |
| M.1    | 6.88                           | 29.2                                 | 46  | 51            | 1               | 2                 | 0                | 5.0                                    | 5.1                     |
| WE-38  | 7.30                           | 34.3                                 | 45  | 52            | 1               | 1                 | 0                | 5.2                                    | 5.1                     |

<sup>a</sup>By Eq. (1).

<sup>b</sup>Recharge NO<sub>3</sub>-N from heavily manured crop rotation land use within subwatershed assumed equal to that from continuous corn, 20 mg l<sup>-1</sup>.

Assuming uniform recharge from all land uses within each subwatershed, the simple model for prediction of  $\text{NO}_3\text{-N}$  concentration at each subwatershed outlet within the larger watershed WE-38 is:

$$\text{NO}_3\text{-N} (\text{mg l}^{-1}) = (1.0) (\% \text{ forest}) + (8.0) (\% \text{ rotation}) + (20.0) (\% \text{ corn}) \\ + (10.0) (\% \text{ pasture}) + (30.0) (\% \text{ animals}) \quad (1)$$

where land use percentages are from Table 2. Heavily manured crop rotation fields within subwatershed W.T4.3 were an exception to application of this basic land use categorization equation; they were assumed to be equivalent to continuous corn in recharge  $\text{NO}_3\text{-N}$  concentration,  $20.0 \text{ mg l}^{-1}$  (Jemison and Fox, 1994). Application of Eq. (1) further assumes that all subwatersheds are at steady state with regard to both flow and water quality, and that streamflow at the outlet of each subwatershed is a summation of all recharge within the subwatershed. This assumption was inferred by the flowpath simulations and substantiated by analysis of the flow data collected at the time of sampling.

Table 2 shows measured  $\text{NO}_3\text{-N}$  concentrations at the subwatershed outlets as well as those calculated by this simple model, while Fig. 6 is a plot of calculated against measured  $\text{NO}_3\text{-N}$  concentrations. The applicability of Eq. (1) at the subwatershed scales

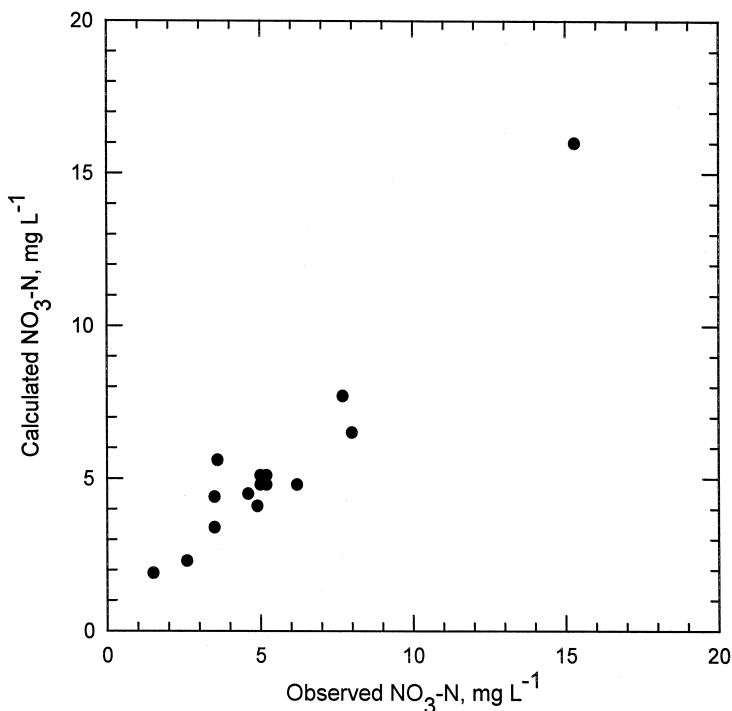


Fig. 6.  $\text{NO}_3\text{-N}$  predicted by Eq. (1) compared to observed values from Table 2; illustration of land use contribution to stream  $\text{NO}_3\text{-N}$  at subwatershed scale.

and land uses it addresses are obvious from the figure. There is an excellent match between observed and calculated values at the lower  $\text{NO}_3\text{-N}$  concentrations ( $< 8$ ) from 14 of the 15 subwatersheds considered, and if the assumption of recharge nitrate concentration from the heavily manured fields within W.T4.3 is appropriate, the equation continues to be applicable up to the range of  $15 \text{ mg l}^{-1} \text{ NO}_3\text{-N}$  which describes the integration of land use effects on stream quality within this particular subwatershed. Overall, the model appears to adequately simulate  $\text{NO}_3\text{-N}$  concentrations for subwatershed areas ranging from nearly 100% forest land use, through all combinations of agricultural land use on the lateral tributary subwatersheds, to the total area of WE-38. The goodness of prediction also suggests that the assumption of small-scale self-contained subsurface flow is appropriate down to the scale of the subwatersheds in Table 2 modeled by Eq. (1).

Obviously, this exercise is not as rigorous as sampling ground water within each of the subwatersheds or other more direct field-based measurements showing the accuracy of the flowpath simulations. But we face this type of problem continually in the areas of watershed hydrology, especially when dealing with subsurface flow systems where intensive sampling is both difficult and expensive. The nitrate calculations we did were indeed simple, but they have not been previously demonstrated at the small subwatershed scales we consider, especially associated with flowpath simulations justifying their use. In the subsurface, resolution generally comes from a variety of observations suggesting similar results. Here, the flowpath simulations developed in a variety of formats suggest the existence of subwatershed-scale subsurface flow systems—a simple analysis of stream nitrate data at the same subwatershed scale suggests that the nitrate concentrations found are related directly to the mix of land use within the subwatershed. Both approaches lead to the same conclusion.

## 8. Implications for land management

Rural upland watersheds of the northeastern USA are generally of mixed land use. Cropped and forested land uses, and sometimes small urban or suburban areas, all contribute to the same flow systems. Contaminants introduced by agriculture are generally 'nonpoint' in nature, and their effects may be manifested at several time and space scales and in more than one watershed flow component. Over the long term, the general flow systems of humid-climate upland watersheds tend to be fixed in space. Outside of major structural modifications, there is minimal opportunity to control or manipulate the hydrology of these ground water-dominated flow systems at a scale large enough to alter the dominant flowpath patterns. Thus, water quality management strategies applied to agriculturally dominated watersheds will likely be nonhydrologic; i.e., change of land use (type and amount), control of agricultural chemical use on specific land uses, and/or guidelines for land use positioning within the watershed.

A major implication of our findings related to watersheds with layered fractured aquifers is that we can inventory land use/land management within subwatersheds, down to perhaps the scale of a second-order stream, integrate total land use inputs of nitrate to ground water within these areas, and translate them directly to long-term loads

and/or average concentrations in nonstorm streamflow. Change in land use within a specific subwatershed to either more or less intensive should translate directly to an increase or decrease, respectively, of nitrate levels in the stream. Further, because of the relatively short travel times found along the ground water flowpaths within these layered fractured flow systems, effects of land use changes on the underlying ground water may be manifested within the ground water body and stream at the scale of months rather than years. However, it must be kept in mind that this conclusion is based heavily on our calibrated values of  $S_y$ .

Altering the mix of land uses and/or levels of management over the entire watershed can be used to achieve target chemical concentrations and/or loads in the stream, but the ground water body is affected differentially by land use positioning. Recharge of the deeper aquifer occurs mainly from the uppermost portions of the watershed land surface (the drainage divides), so control of nitrogen loss from the root zone in these areas is critical to protecting water quality within the deeper aquifer and minimizing long-term low-level contamination of the stream. Control can be exerted either by managing chemical inputs to the soil or by restricting the type of land use allowed in these areas. Further, we must recognize the sensitivity of water quality within the deeper aquifer to positioning of land use over this part of the flow system. Simulation results for cross-section configurations typical of WE-38 show that moving an intensive land use only tens of meters from the divide will dramatically reduce nitrate concentrations within the deeper aquifer, while affecting the shallower portions of the subsurface flow system downgradient only minimally. Water quality within the shallow fracture zone in positions downslope from the recharge areas is controlled directly by overlying and immediately upgradient land uses, and only indirectly by water reemerging from the deeper aquifer because of the dominant lateral or upward flowpaths over this part of the watershed. Thus, contamination of the deeper aquifer is insensitive to land use in these positions.

## 9. Summary

For the watershed and aquifer conditions considered here, flowpath simulations suggest the existence of self-contained ground water flow systems at the subwatershed scale. These findings are supported by nitrate concentrations measured in baseflow over the watershed. The flowpath simulations alone show both the potential for contamination of ground water and nonstorm streamflow by agricultural land use distribution, as well as the possibility to minimize contamination of targeted portions of the subsurface flow system by controlling land use position. As importantly perhaps, the flowpath simulation methodology developed and presented here provides a framework with which to develop, test, and evaluate more detailed water quality investigations within WE-38 and watersheds having similar layered and fractured aquifers.

Where all components of the hydrologic cycle are closely connected, as in the humid Northeast, land management and planning schemes having water quality objectives must incorporate knowledge of the generalized ground water flow system. Management strategies must be developed in context of the interactions between land use position,

ground water movement and associated contaminant transport, and streamflow produced by ground water discharge, combined with recognition of the space and time scales of concern. In the layered fractured aquifers considered here, depths and areal extents of the characteristic fracture layers, their hydraulic conductivity and porosity distributions, subsurface watershed boundaries, and locations of the dominant ground water flow units of recharge, lateral flow, and discharge must all be considered when defining these interactions.

## Acknowledgements

Contribution from the U.S. Department of Agriculture, Agricultural Research Service, in cooperation with the Pennsylvania Agricultural Experiment Station, the Pennsylvania State University, University Park, PA, USA.

## References

- Cline, G.D., 1968. Geologic factors influencing well yields in a folded sandstone–siltstone–shale terrain within the East Mahantango Creek Watershed. MSc Thesis, Pennsylvania State University, University Park, PA.
- EPA, 1983. Chesapeake Bay: A framework for action. USEPA, Philadelphia, PA.
- EPA, 1996. Environmental indicators of water quality in the United States. EPA 841-R-96-002. USEPA, Washington, DC.
- Ferguson, H.F., 1967. Valley stress relief in the Allegheny Plateau. *Assn. Eng. Geol. Bull.* 4, 63–68.
- Gburek, W.J., Urban, J.B., Schnabel, R.R., 1986. Nitrate contamination of ground water in an upland Pennsylvania watershed. *Proceedings of Agricultural Impacts on Ground Water—A Conference*. NWWA, Omaha, NE, pp. 352–380.
- Gburek, W.J., Urban, J.B., 1990. The shallow weathered fracture layer in the near-stream zone. *Ground Water* 28, 875–883.
- Gburek, W.J., Urban, J.B., Schnabel, R.R., 1991. Effects of agricultural land use on contaminant transport in a layered fractured aquifer. In: *Nachtnebel, H.P., Kovar, K. (Eds.), Hydrological Basis of Ecologically Sound Management of Soil and Groundwater*. IAHS Pub. No. 202, pp. 33–42.
- Gburek, W.J., Folmar, G.J., Urban, J.B., 1998. Field data and ground water modeling in a layered fractured aquifer. *Ground Water*, in press.
- Gerhart, J.M., 1984. A model of regional ground-water flow in secondary-permeability terrane. *Ground Water* 22, 168–175.
- Golden Software, 1995. *SURFER Version 6 User's Manual*. Golden Software, Golden, CO.
- Jemison, J.M., Fox, R.H., 1994. Nitrate leaching from nitrogen-fertilized and manured corn measured with zero-tension pan lysimeters. *J. Environ. Qual.* 23, 337–343.
- Khaleel, R., 1989. Scale dependence of continuum models for fractured basalts. *Water Resour. Res.* 25, 1847–1855.
- Lee, R.R., Kettle, R.H., Bownds, J.M., Rizk, T.A., 1992. Aquifer analysis and modeling in a fractured, heterogeneous medium. *Ground Water* 30, 589–597.
- Long, J.C.S., Remer, J.S., Wilson, C.R., Witherspoon, P.A., 1982. Porous media equivalents for networks of discontinuous fractures. *Water Resour. Res.* 18, 648–658.
- McDonald, M.G., Harbaugh, A.W., 1988. A modular three-dimensional finite-difference ground-water flow model. *Techniques of Water-Resources Investigations*. Book 6, Chap. 1.
- Owens, L.B., Edwards, W.M., VanKeuren, R.W., 1994. Groundwater nitrate levels under fertilized grass and grass-legume pastures. *J. Environ. Qual.* 23, 752–758.

- Peters, R.R., Klavetter, E.A., 1988. A continuum model for water movement in an unsaturated fractured rock mass. *Water Resour. Res.* 24, 416–430.
- Pionke, H.B., Urban, J.B., 1985. Effects of agricultural land use on ground-water quality in a small Pennsylvania watershed. *Ground Water* 23, 68–80.
- Pionke, H.B., Gburek, W.J., Sharpley, A.N., Schnabel, R.R., 1996. Flow and nutrient export patterns for an agricultural hill-land watershed. *Water Resour. Res.* 32, 1795–1804.
- Pollock, D.W., 1989. Documentation of computer programs to compute and display pathlines using results from the U.S. Geological Survey modular three-dimensional finite-difference ground-water flow model. USGS Scientific Software Group, Washington, DC.
- Schnabel, R.R., Urban, J.B., Gburek, W.J., 1993. Hydrologic controls in nitrate, sulfate, and chloride concentrations. *J. Environ. Qual.* 22, 589–596.
- Scholefield, D., Tyson, K.C., Garwood, E.A., Armstrong, A.C., Hawkins, J., Stone, A.C., 1993. Nitrate leaching from grazed grass lysimeters: effects of fertilizer input, field drainage, age of sward and patterns of weather. *J. Soil Sci.* 44, 601–613.
- Selim, H.M., 1987. Water seepage through multilayered anisotropic hillside. *Soil Sci. Soc. Am. J.* 51, 9–16.
- Toth, J., 1963. A theoretical analysis of ground water flow in small drainage basins. *J. Geophys. Res.* 68, 4795–4812.
- Trexler, J.P., 1964. The geology of Klingerstown, Valley View and Lykens Quadrangles, Southern Anthracite Field, Pennsylvania. PhD Thesis, The University of Michigan, Ann Arbor, MI.
- Urban, J.B., 1977. The Mahantango Creek watershed—evaluating the shallow ground water regime. In: Correll, D.L. (Ed.), *Watershed Research in Eastern North America*. Smithsonian Institute, Washington, DC, pp. 251–275.
- Urban, J.B., Pasquarell, G.C., 1992. Combining well packer tests and seismic refraction surveys for hydrologic characterization of fractured rock. Proceedings, Sixth Outdoor Action Conference on Aquifer Restoration, Ground Water Monitoring and Geophysical Methods. National Ground Water Association, pp. 645–654.
- Waterloo Hydrogeologic, 1996. Visual MODFLOW Version 2.00 User's Manual. Waterloo Hydrogeologic, Waterloo, Ontario, Canada.
- Wyrick, G.G., Borchers, J.W., 1981. Hydrologic effects of stress relief fracturing in an Appalachian valley. USGS Water Supply Paper 2177, 51 pp.